Smooth GaN membranes by polarization-assisted electrochemical etching

Downloaded from: https://research.chalmers.se, 2026-04-04 13:10 UTC

Citation for the original published paper (version of record):

Ciers, J., Bergmann, M., Hjort, F. et al (2021). Smooth GaN membranes by polarization-assisted electrochemical etching. Applied Physics Letters, 118(6). http://dx.doi.org/10.1063/5.0034898

N.B. When citing this work, cite the original published paper.

research.chalmers.se offers the possibility of retrieving research publications produced at Chalmers University of Technology. It covers all kind of research output: articles, dissertations, conference papers, reports etc. since 2004. research.chalmers.se is administrated and maintained by Chalmers Library

(article starts on next page)

Applied Physics Letters ARTICLE scitation.org/journal/apl

Smooth GaN membranes by polarization-assisted electrochemical etching

Cite as: Appl. Phys. Lett. **118**, 062107 (2021); doi: 10.1063/5.0034898
Submitted: 23 October 2020 · Accepted: 20 January 2021 ·
Published Online: 11 February 2021

View Online

Export Citation

CrossMark

J. Ciers,[1,a)] M. A. Bergmann,[1] F. Hjort,[1] J.-F. Carlin,[2] N. Grandjean,[2] and Å. Haglund[1]

AFFILIATIONS

[1]Department of Microtechnology and Nanoscience, Chalmers University of Technology, 41296 Gothenburg, Sweden
[2]Institute of Physics, École Polytechnique Fédérale de Lausanne (EPFL), 1015 Lausanne, Switzerland

[a)]Author to whom correspondence should be addressed: joachim.ciers@chalmers.se

ABSTRACT

III-nitride membranes offer promising perspectives and improved device designs in photonics, electronics, and optomechanics. However, the removal of the growth substrate often leads to a rough membrane surface, which increases scattering losses in optical devices. In this work, we demonstrate membranes with etched surface roughness comparable to that of the as-grown epitaxial material, accomplished by the implementation of a properly designed built-in polarization field near the top of the sacrificial layer from an AlInN interlayer, which is polarization-mismatched to GaN. This leads to a steeper reduction in free carrier density during the electrochemical etching of the sacrificial layer, limiting the etching current and thus causing an abrupter etch stop. As a result, the root mean square roughness is reduced to 0.4 nm over $5 \times 5\ \mu m^2$. These smooth membranes open attractive pathways for the fabrication of high-quality optical cavities and waveguides operating in the ultraviolet and visible spectral regions.

© 2021 Author(s). All article content, except where otherwise noted, is licensed under a Creative Commons Attribution (CC BY) license (http://creativecommons.org/licenses/by/4.0/). https://doi.org/10.1063/5.0034898

The III-nitride (III-N) family is the most widely used group of wide-bandgap semiconductors, essential for the realization of ultraviolet and visible light emitters[1,2] and high electron mobility transistors (HEMTs).[3] However, due to a large lattice mismatch with other semiconductors, heterogeneous epitaxy of III-Ns is compromised,[4] resulting in large dislocation densities ($10^8 - 10^{10}$ cm^{-2}) and thus reduced material quality. This issue can be partially overcome through the growth of thick buffer layers over 1 μm,[4] but in some cases, this is not possible or desirable. For example, the channel of a HEMT (where most heat is generated) should ideally be in close proximity to a material with excellent thermal conductivity, such as diamond or copper. Moreover, optical cavities and waveguides require high-quality core materials embedded in a low refractive index material for optical confinement. In the III-N material family, the large lattice mismatch between the binary compounds inherently limits the achievable refractive index contrast of a bilayer in order to keep the layers pseudomorphic. As a consequence, the optical confinement provided by epitaxially grown layers is thereby limited,[2,5] and the realization of distributed Bragg reflectors (DBRs) in AlInN/(Al)GaN or AlGaN/GaN requires a large number of pairs, which might be detrimental for practical use.[6,7] The issues with heterogeneous epitaxy of III-Ns can be circumvented by lifting-off III-N membranes from the growth substrate and then bonding them to the material of choice. This approach is especially advantageous when the membrane can be grown on a lattice-matched substrate rather than on the often lattice-mismatched or even the amorphous material that the III-N structure is to be integrated with. Various techniques have been used to separate membranes from their growth substrate, such as thermal decomposition of GaN,[8] laser liftoff,[9] photoelectrochemical etching,[10] and electrochemical (EC) etching.[11,12] Also reported are III-N growth on Si,[13] SiC,[14] or Nb_2N,[15] followed by wet or dry etching to remove the substrate and growth on two-dimensional (2D) van der Waals materials such as boron nitride, followed by mechanical transfer.[16] Among these, only EC etching simultaneously allows for the fabrication of membranes with low dislocation density (when grown on a lattice-matched substrate), precisely controlled thickness (hard to control with laser liftoff), smooth surfaces (challenging to obtain with laser liftoff), and etching rates up to 1 μm/s (photoelectrochemical etching is notably slower), while being compatible with electrical contacts [the thermal decomposition of GaN is not, due to the high temperatures required, >1000 °C (Ref. 8)].

A smooth membrane surface is paramount to achieving optical cavities with a high *Q*-factor, and a precise thickness control is highly desirable to match the cavity resonance to the optical gain, both

leading to low lasing thresholds. Unfortunately, the root mean square (RMS) roughness is often a limiting factor and typically in excess of 1 nm for GaN membranes on their backside, i.e., where the substrate is removed, using EC etching[11,17–19] as well as for many other techniques.[9,13,20] The lowest reported etched surface roughness values are for growth on Si (0.6 nm RMS over $0.5 \times 0.5\ \mu m^2$)[21] and photoelectrochemical etching (0.65 nm over $10 \times 10\ \mu m^2$ and 0.25 nm over $1 \times 1\ \mu m^2$).[10,22]

The EC etching of GaN relies on the generation of holes (corresponding to broken chemical bonds) in the GaN valence band (VB) near the GaN/electrolyte interface to overcome the chemical resistance of GaN. This occurs when a sufficiently large potential difference is applied over the GaN/electrolyte interface, which behaves as a Schottky barrier with a variable height[23] so that the VB is above or at least near the Fermi level (E_F) at the interface. In practice, this means that the potential difference over this interface should be at least equal to the GaN bandgap of 3.4 eV.[23]

In this work, the focus has been to reduce the roughness of electrochemically etched GaN surfaces by exploring the implementation of polarization fields near the etching interface (marked in red in Fig. 1).

The samples were grown by metal-organic vapor-phase epitaxy on a Ga-polar GaN-on-sapphire template. The sample structures are sketched in Fig. 1. The membranes are grown on a 100 nm Si-doped GaN sacrificial layer with various donor concentrations N_D on top of a 100 nm n-doped GaN current spreading layer ($N_D = 3 \times 10^{18}$ cm^{-3}). The membrane layer structure is representative for what is typically used in blue-emitting electrically injected LEDs or vertical-cavity surface-emitting lasers (VCSELs) and are detailed in the supplementary material, Note 1. Different interlayers (ILs) are grown in between the sacrificial layer and the membrane layers to tailor the built-in polarization and thereby study the effect of the polarization-induced electric field on the membrane etching. Samples of type I contain no IL, samples of type II contain a 20 nm $Al_{0.2}Ga_{0.8}N$ IL, and samples of type III contain a 20 nm $Al_{0.82}In_{0.18}N$ IL. In both cases II and III, 1 nm of AlN was inserted between the sacrificial layer and the interlayer to minimize alloy disorder at the interface. These interlayers introduce a built-in electric field of around 1 MV/cm for type II and 4 MV/cm for type III in the absence of any screening.[24] Note that the type II IL adds strain, while the type III IL is nearly lattice-matched to the rest of the structure.[25] Therefore, a type II structure could lead to a reduction in material quality of the subsequently grown layers. However, in the present type II samples, no deterioration was observed in x-ray diffraction measurements.

The samples were prepared for EC etching by (i) etching via-holes (10 μm diameter) to expose the sacrificial layer laterally to the electrolyte, (ii) depositing an Al contact (1.5 mm diameter) to apply a bias voltage during EC etching, and (iii) adding photoresist protection to the top surface, as sketched in Fig. 1. When the top surface is left unprotected during EC etching, we observe vertical parasitic etching on separate locations, likely originating at dislocations.[26]

EC etching was performed in nitric acid while applying a constant positive potential to the sample, with respect to a graphite counter electrode. The created membranes were exfoliated onto a Si carrier using double-sided tape, with the N-polar surface facing upwards, allowing for characterization with atomic force microscopy (AFM) and scanning electron microscopy (SEM). Further experimental details are given in the supplementary material, Note 1.

Depending on etching voltage and doping concentration in the sacrificial layer, three different etching regimes can be distinguished as shown in Fig. 2.[12,17] For low voltages or low doping concentrations, no etching takes place, as the voltage drop over the GaN/electrolyte interface is too low to generate holes at this interface. For high voltages and/or high doping concentrations, this voltage drop is large enough over the entire interface, and the sacrificial layer is completely etched. For intermediate voltages and doping concentrations, the voltage drop is too small over most of the interface but is enhanced by local fluctuations in the morphology or composition, leading to porous etching. Figures S1(a) and S1(b) in the supplementary material shows the cross section of two samples where the sacrificial layer underwent porous etching in one and complete etching in the other. It should be noted

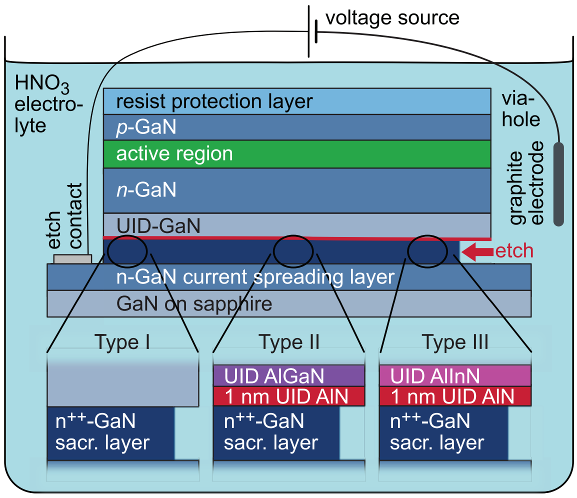

FIG. 1. Sketch of the three sample types. The interface between the membrane and the sacrificial layer, which becomes the etched membrane surface after EC etching, is the main focus of this work and is marked in red.

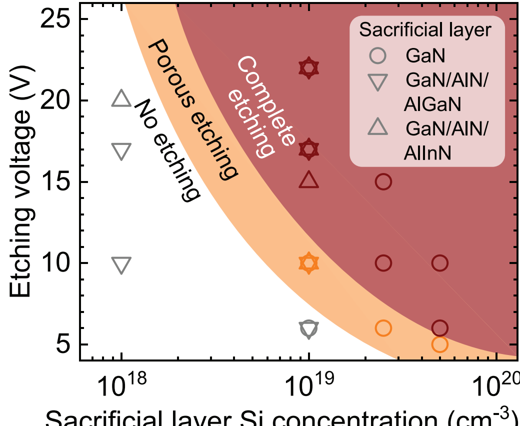

FIG. 2. The different etching regimes as a function of etching voltage and donor concentration in the sacrificial layer.

© Author(s) 2021

that not only the sacrificial layer but also all membrane layers were exposed to the electrolyte in the holes, as shown in Fig. 1. This resulted in porous etching of the *n*-GaN membrane layer for etching voltages above 10 V. No etching or porosification was observed in the other membrane layers for etching voltages up to 22 V. Porosification of *n*-GaN can be avoided by either lowering the doping concentration of this layer or protecting it with resist or a dielectric coating during etching. However, dislocations that act as vertical etching channels can also lead to porosification of the n-GaN as seen in Figs. 4(j)–4(l).

The applied voltage or doping concentration required for a transition from no etching to porosification, or from porosification to complete etching, is the same for samples of types I, II, and III. This is because the polarization field is screened by the free carriers in most of the sacrificial layer. It only has an effect within the topmost few tens of nm of the sacrificial layer. No preferential lateral etching was observed near the top of the sacrificial layer, i.e., the etch was homogeneous over the entire sacrificial layer thickness for all three sample types, as illustrated in Fig. S1(c) in the supplementary material.

When implementing a built-in polarization field near the top of the sacrificial layer, the etching reaction will be stopped much more abruptly along the growth direction, resulting in a smoother etched surface. This can be understood by observing the band structure of the samples in Figs. 3(a)–3(d). These data were calculated with Nextnano[27] using the piezoelectric polarization parameters from

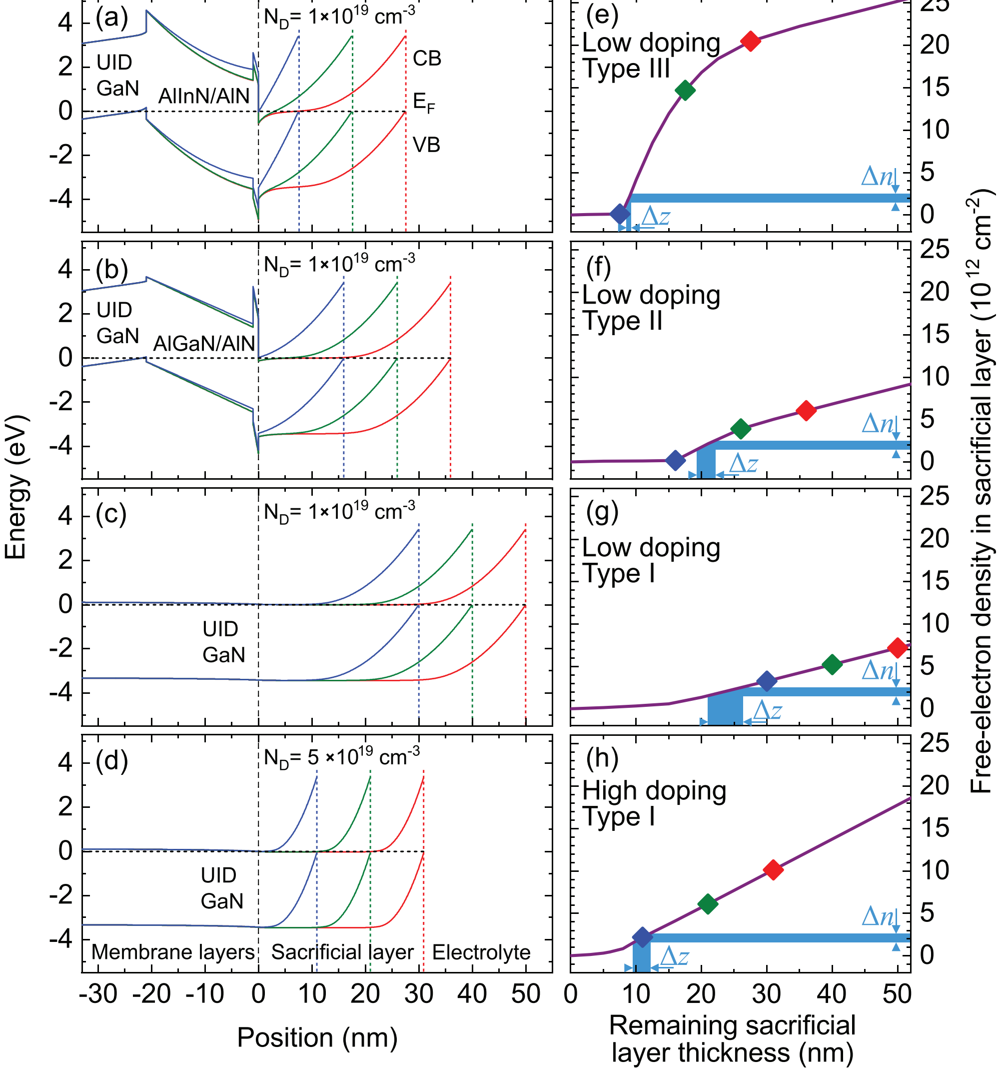

FIG. 3. Evolution of the band structure and free-electron density in the sacrificial layer during the etching process. (a)–(d) Band structure along the *c*-axis for different sample types and doping concentrations. For every case, the band structure is plotted for three different remaining thicknesses of the sacrificial layer in red, green, and blue. (e)–(h) The total free-electron density in the sacrificial layer (integrated over *z*), as a function of the remaining sacrificial layer thickness, for the same sample structures as in (a)–(d). The squares show the electron density for the band structures plotted in (a)–(d) in the corresponding color. The decrease in remaining sacrificial layer thickness (Δz), which results in a reduction in electron density (Δn) from 2.5 to 1.5 $\times 10^{12}$ cm^{-2}, is highlighted in light blue. This Δz gives a qualitative indication of the expected surface roughness.

© Author(s) 2021

Ambacher *et al.*[24] In these calculations, the GaN/electrolyte interface is modeled as a Schottky barrier. Note that, even though in reality the electron and hole quasi-Fermi levels will not coincide when a potential is applied across this interface, the band curvature is fully taken into account by the Schottky boundary condition, without the need to apply an additional bias. Therefore, both quasi-Fermi levels and E_F coincide and are constant throughout the sample in this model. As explained above, the etching reaction can only take place when a sufficiently large potential difference occurs over the GaN/electrolyte interface. In this case, holes are generated in the depleted GaN and accumulate at the interface. However, as the sacrificial layer thickness is reduced during etching, the 2D free-electron density in the remaining sacrificial layer (i.e., the free-electron density integrated over the growth direction z) is reduced, increasing the resistivity and decreasing the potential difference over the GaN/electrolyte interface. The reaction will, thus, drastically slow down when the electron density in the remaining sacrificial layer is reduced. This roughly occurs when the sacrificial layer thickness is so small that it just still allows the VB to be (nearly) degenerate at the GaN/electrolyte interface, while the conduction band (CB) is (nearly) degenerate deeper into the layer. This limit situation is shown in blue for all sample structures in Figs. 3(a)–3(d). Both the introduction of a polarization field and the increase in the doping concentration in the sacrificial layer will (i) reduce this remaining thickness limit and (ii) result in a fast drop in electron density with remaining sacrificial layer thickness, as shown in Figs. 3(e)–3(h). The effect (ii) leads to a much better defined etch stop and therefore a smoother surface. Both effects are much stronger with the implementation of a strong polarization field than what can be achieved with the increased doping concentration, leading to very smooth surfaces for a sufficiently strong polarization field, as will be demonstrated below. This is a result of the triangular-shaped potential introduced by the polarization field, as can be seen in Fig. 3(a), and to a lesser extent, in Fig. 3(b). This region contains a high density of free electrons (on the order of 10^{13} cm^{-2} for the type III sample with an AlInN-based IL). This results in an excellent conductivity of the sacrificial layer, even down to a remaining thickness of 10 nm, leading to a small residual sacrificial layer thickness after etching. Additionally, when such a triangular-shaped potential is moved up with respect to the Fermi level (becoming less degenerate), its contained electron density is quickly reduced, causing the EC etching to stop abruptly. To illustrate this effect, the decrease in remaining sacrificial layer thickness (Δz), which results in an electron density reduction (Δn) from 2.5 to 1.5×10^{12} cm^{-2} (corresponding to the steepest decrease in electron density as a function of remaining sacrificial layer thickness in all samples), is highlighted in light blue in Figs. 3(e)–3(h). Δz gives a qualitative indication of the distance over which the EC etching reaction is stopped. Small values of Δz will lead to a small roughness. Comparison of Δz values displayed in Figs. 3(e)–3(h) clearly shows that an etched surface of a type III sample is expected to be much smoother than what can be achieved by high doping concentrations in the sacrificial layer. This will be confirmed by the experimental results below.

The effect of increasing sacrificial layer doping on the etched surface roughness is illustrated in Figs. 4(a)–4(f). Two manifestations of roughness are observed: (i) dots of the remaining sacrificial layer material, which are a few hundred nm wide and a few tens of nm thick, and (ii) background roughness of the fully etched regions. When increasing the sacrificial layer donor concentration, the dot density does not monotonically decrease, and the background roughness remains relatively high, around several nm RMS roughness over a 5×5 μm^2 AFM scan. Elevated doping concentrations lead to a rough growing surface and thus also to a poor morphology of the etched surface. To minimize this effect, the higher-doped type I samples ($N_D > 1 \times 10^{19}$ cm^{-3}) were modulation doped, but the sample with the highest doping still suffered from a deteriorate morphology of the etched surface as seen in Figs. 4(c) and 4(f). It should be noted that the etch voltage was carefully chosen to be just above the threshold for complete electrochemical etching to avoid excess roughness induced by a too high etching rate, as discussed in supplementary material, Note 2, and is shown in Fig. S2. As such, the etching speed of all samples shown in Fig. 4 is similar, varying between 0.4 and 1.1 μm/s.

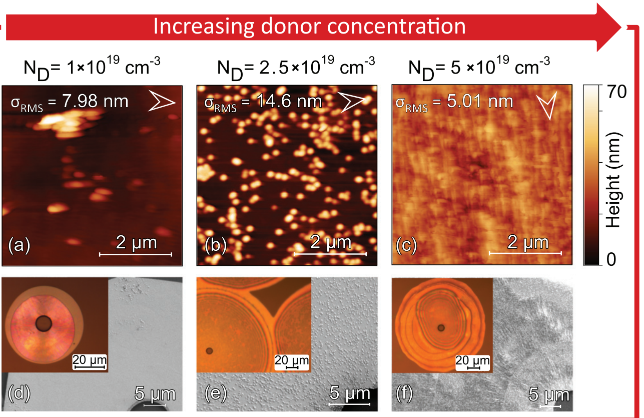

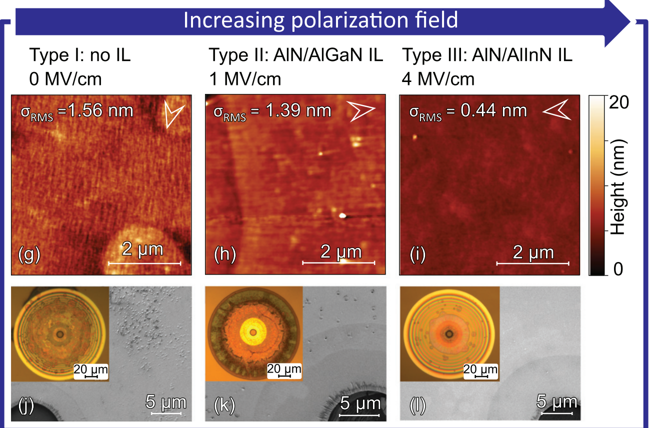

FIG. 4. Evolution of the RMS roughness σ_{RMS} of the etched surface. The upper half (a)–(f) shows this surface as a function of doping concentration in the sacrificial layer, for samples of type I, etched in 0.3 M HNO_3. The lower half (g)–(l) shows the surface as a function of polarization field, for a sacrificial layer doping concentration of 1×10^{19} cm^{-3}, etched in 0.1 M HNO_3. (a)–(c) and (g)–(i) AFM scans over 5×5 μm^2 on the etched N-polar surface of exfoliated membranes. The arrowhead indicates the etching direction. (d)–(f) and (j)–(l) SEM images of the etched surfaces. The via-hole can be observed in the center of each membrane. Inset: optical microscopy images of the etched membranes before exfoliation. The samples were etched using voltages of (a) and (d) 17 V, (b) and (e) 10 V, (c) and (f) 6 V, and (g)–(l) 17 V.

© Author(s) 2021

When increasing the polarization field instead of the doping concentration [Figs. 4(g)–4(l)], both the density of dots and the background roughness are reduced. For type III, the RMS roughness is 0.4 nm over $5 \times 5\ \mu m^2$, a record-low etched surface roughness for an electrochemically etched sample. This surface is as smooth as the best results demonstrated by photoelectrochemical etching[10,22] or III-N growth on Si followed by selective etch of Si.[21] Moreover, it is comparable to the surface roughness of the as-grown top surface of the samples (Fig. S3 in the supplementary material). The smooth etched surface leads to clear interference fringes when illuminated in an optical microscope [Fig. 4(l) (inset)], a clear illustration of the high optical quality. These fringes are not due to a membrane thickness variation but rather to a change in air-gap thickness as the membrane buckles up by a few μm in the center after release, as a result of residual strain. Furthermore, the fringes are very symmetrical as a result of an isotropic and homogeneous etching. The high free-electron density and excellent conductivity of the sacrificial layer in this structure [as shown in Fig. 3(e)] induce this high isotropy. The other samples, with poorer sacrificial layer conductivity, exhibit a less isotropic etch, as can be seen by comparing the insets of Figs. 4(d)–4(f) and 4(j)–4(l).

The etched surface morphology may also depend upon the electrolyte concentration, and therefore, two HNO_3 concentrations were tested,[28] 0.1 and 0.3 M. The results can be seen by comparing Figs. 4(a) and 4(d) with Figs. 4(g) and 4(j) as these two samples are identical on all parameters except for the electrolyte concentration. The SEM images in Figs. 4(d) and 4(j) show a very similar morphology, with a large variation of residual dot density over the membrane. The AFM images [Figs. 4(a) and 4(g)] show a different morphology, but this is due to the much higher local dot density in the area of the former compared to the latter. Overall, no significant difference in etching speed (the progress of the etch front) or the final morphology of the etched surfaces was observed. This indicates that the etching process is not limited by the electrolyte concentration with the present parameters but rather by sample conductivity and the availability of holes at the GaN/electrolyte interface. This observation is coherent with the explanation of the improved smoothness of membranes featuring a built-in polarization field given above.

We have demonstrated that the surface roughness of the etched N-polar surface of GaN membranes created by electrochemical liftoff can be drastically reduced through the implementation of a polarization field. With a properly designed polarization field, the free carrier density in the sacrificial layer reduces more abruptly within the remaining sacrificial layer thickness, leading to a sharper etch stop and thus a much smoother etched surface. The smoothest surface was obtained by using an AlInN-based interlayer lattice-matched to GaN, resulting in an RMS roughness of about 0.4 nm, which is the best achieved by electrochemical etching and comparable to the roughness of the as-grown top surface. These smooth membranes are promising for the fabrication of low-loss optical waveguides and high-quality-factor optical cavities, such as photonic crystals or microcavities with two dielectric DBRs, since they can be grown strain-free on freestanding GaN substrates for an optimal material quality.

See the supplementary material for experimental details on sample growth, processing, and characterization, as well as cross-sectional SEM images, SEM images showing the impact of elevated etching voltages, and AFM scans of the as-grown surface.

This work was performed in part at Myfab Chalmers, and the project was financially supported by the European Research Council (ERC) under the European Union's Horizon 2020 research and innovation program (Grant Agreement No. 865622) and the Swedish Research Council (Grant Agreement No. 2018-00295).

DATA AVAILABILITY

The data that support the findings of this study are available from the corresponding author upon reasonable request.

REFERENCES

[1] S. Nakamura, T. Mukai, and M. Senoh, Appl. Phys. Lett. **64**, 1687 (1994).
[2] S. Nakamura, M. Senoh, S. Nagahama, N. Iwasa, T. Yamada, T. Matsushita, H. Kiyoku, and Y. Sugimoto, Jpn. J. Appl. Phys., Part 2 **35**, L74 (1996).
[3] M. A. Khan, A. Bhattarai, J. N. Kuznia, and D. T. Olson, Appl. Phys. Lett. **63**, 1214 (1993).
[4] O. Ambacher, J. Phys. D **31**, 2653 (1998).
[5] J. Ciers, J. G. Roch, J.-F. Carlin, G. Jacopin, R. Butté, and N. Grandjean, Phys. Rev. Appl. **7**, 034019 (2017).
[6] X. H. Zhang, S. J. Chua, W. Liu, L. S. Wang, A. M. Yong, and S. Y. Chow, Appl. Phys. Lett. **88**, 191111 (2006).
[7] G. Cosendey, A. Castiglia, G. Rossbach, J.-F. Carlin, and N. Grandjean, Appl. Phys. Lett. **101**, 151113 (2012).
[8] R. Tao, M. Arita, S. Kako, and Y. Arakawa, Appl. Phys. Lett. **103**, 201118 (2013).
[9] L. Tang, Y. Wang, G. Cheng, M. J. Manfra, and T. D. Sands, MRS Proc. **1432**, g03 (2012).
[10] R. Jayaprakash, F. G. Kalaitzakis, M. Kayambaki, K. Tsagaraki, E. Monroy, and N. T. Pelekanos, J. Mater. Sci. **49**, 4018 (2014).
[11] S. H. Park, G. Yuan, D. Chen, K. Xiong, J. Song, B. Leung, and J. Han, Nano Lett. **14**, 4293 (2014).
[12] M. A. Bergmann, J. Enslin, R. Yapparov, F. Hjort, B. Wickman, S. Marcinkevičius, T. Wernicke, M. Kneissl, and Å. Haglund, Appl. Phys. Lett. **115**, 182103 (2019).
[13] N. Vico Triviño, R. Butté, J.-F. Carlin, and N. Grandjean, Nano Lett. **15**, 1259 (2015).
[14] B. K. SaifAddin, A. Almogbel, C. J. Zollner, H. Foronda, A. Alyamani, A. Albadri, M. Iza, S. Nakamura, S. P. DenBaars, and J. S. Speck, Semicond. Sci. Technol. **34**, 035007 (2019).
[15] D. J. Meyer, B. P. Downey, D. S. Katzer, N. Nepal, V. D. Wheeler, M. T. Hardy, T. J. Anderson, and D. F. Storm, IEEE Trans. Semicond. Manuf. **29**, 384 (2016).
[16] T. Ayari, S. Sundaram, X. Li, Y. E. Gmili, P. L. Voss, J. P. Salvestrini, and A. Ougazzaden, Appl. Phys. Lett. **108**, 171106 (2016).
[17] Y. Zhang, S.-W. Ryu, C. Yerino, B. Leung, Q. Sun, Q. Song, H. Cao, and J. Han, Phys. Status Solidi B **247**, 1713 (2010).
[18] D. Chen and J. Han, Appl. Phys. Lett. **101**, 221104 (2012).
[19] A. W. Bruch, K. Xiong, H. Jung, X. Guo, C. Zhang, J. Han, and H. X. Tang, Appl. Phys. Lett. **110**, 021111 (2017).
[20] S. Lee, S. Mishkat-Ul-Masabih, J. T. Leonard, D. F. Feezell, D. A. Cohen, J. S. Speck, S. Nakamura, and S. P. DenBaars, Appl. Phys. Express **10**, 011001 (2017).
[21] I. Rousseau, I. Sánchez-Arribas, K. Shojiki, J.-F. Carlin, R. Butté, and N. Grandjean, Phys. Rev. B **95**, 125313 (2017).
[22] A. S. Abbas, A. Y. Alyamani, S. Nakamura, and S. P. Dembaars, Appl. Phys. Express **12**, 036503 (2019).
[23] C. Zhang, G. Yuan, A. Bruch, K. Xiong, H. X. Tang, and J. Han, J. Electrochem. Soc. **165**, E513 (2018).
[24] O. Ambacher, J. Majewski, C. Miskys, A. Link, M. Hermann, M. Eickhoff, M. Stutzmann, F. Bernardini, V. Fiorentini, V. Tilak, B. Schaff, and L. F. Eastman, J. Phys. **14**, 3399 (2002).
[25] J.-F. Carlin and M. Ilegems, Appl. Phys. Lett. **83**, 668 (2003).
[26] F. C.-P. Massabuau, P. H. Griffin, H. P. Springbett, Y. Liu, R. V. Kumar, T. Zhu, and R. A. Oliver, APL Mater. **8**, 031115 (2020).
[27] S. Birner, T. Zibold, T. Andlauer, T. Kubis, M. Sabathil, A. Trellakis, and P. Vogl, IEEE Trans. Electron. Devices **54**, 2137 (2007).
[28] D. Chen, H. Xiao, and J. Han, J. Appl. Phys. **112**, 064303 (2012).

© Author(s) 2021